Invariant activity sequences across the mouse brain

Célian Bimbard[1]*, Kenneth D Harris[2], and Matteo Carandini[1]

[1]UCL Institute of Ophthalmology, University College London, London, United Kingdom
[2]UCL Queen Square Institute of Neurology, University College London, London, United Kingdom

*Correspondence: c.bimbard@ucl.ac.uk

Abstract

An ambition of neuroscience is to identify fundamental patterns of neural activity that are shared across the brain. Such patterns may occur in the cerebral cortex, where neurons are coupled to the population and fire in 50-100 ms sequences. Here we show that these sequences are stable over time and ubiquitous across the brain. Chronic Neuropixels recordings in mouse visual cortex revealed that each neuron was coupled to the local population with a characteristic strength and delay. Stimulus responses formed a sequence where neuronal participation depended on tuning, but delay was fixed. This sequence interacted multiplicatively with the rate code, appeared even during spontaneous activity, and remained stable for weeks. Brainwide Neuropixels recordings revealed that the sequences occur across the entire mouse brain and are often synchronized across regions. These results reveal a stable scaffold for brainwide activity and suggest that the sequences support a canonical computation operating across the brain.

Introduction

The joint activity of populations of neurons is highly structured[1-6]. In principle, neural codes might be extremely complex, and understanding their structure might require characterising the correlation between every pair of neurons[7]. In practice, however, in the cerebral cortex a substantial fraction of this structure can be understood by the relation of each neuron with the summed activity of the local population[8,9]. Each neuron's coupling to the population can be characterized by two numbers. First, the strength of the coupling[8]: while some neurons ("soloists") are weakly coupled to the population, many others ("choristers") show strong coupling. Second, the timing of the coupling: some neurons tend to fire slightly before their peers ("leaders[10]") while others fire after ("followers[11]").

The diversity of coupling delays has the consequence that populations of cortical neurons fire in sequences lasting 50-100 ms. Such sequences occur in the spontaneous activity of the rat somatosensory[2,12] and auditory[2] cortex. In auditory cortex, moreover, the same sequences are seen during responses to tones[2]. Similar sequences of evoked activity have been reported in the rat[13] and mouse[14] visual cortex. The sequences are also seen in the 3-layered cortex of turtles[11], the visual cortex of marmosets[14], and the middle temporal cortex of humans[15,16]. This suggests that such sequences may form a canonical pattern of activity in neural networks, acting as an invariant scaffold for local and global computations.

However, it is not known whether these sequences of activity are localized or distributed. The sequences have been observed in some cortical areas (usually sensory), but it is not known if they extend to regions outside the cortex. Moreover, it is not known whether these sequences are stable or can change over time. Some attributes of cortical responses, such as the spiking statistics or the correlation patterns, remain constant over many days[17,18]. Other properties, such as selectivity for stimuli, appear to change gradually over time, describing a "representational drift" that has been observed in multiple cortical areas[19-25] (but see Refs. [26-31]). Are the 50-100 ms sequences of activity reliable and stable over time?

Here we addressed these issues through a combination of chronic Neuropixels recordings focused on the mouse visual cortex and acute Neuropixels recordings covering an entire hemisphere of the mouse brain. The first set of experiments revealed that the sequences of activity coexist with the firing rate code used to represent stimuli, and that both the diverse population coupling seen across neurons and the arrangement of neuronal activity in sequences remain fixed over weeks. The second set of experiments revealed that these key aspects of the structure of population activity are canonical across the brain and shape the structure of brainwide neural activity.

Results

To investigate the sequences of activity, we first focused on the visual cortex, where we could readily drive neuronal populations through visual stimulation. We inserted Neuropixels 2.0 probes[32] chronically[33] in the visual cortex (VIS) of mice, and recorded from hundreds of neurons over several weeks. We presented a battery of the same 112 contrast-normalized images on each recording day[32], and tracked the same cells across recordings for weeks using UnitMatch[18] (**Figure 1**a).

The responses of individual VIS neurons to different images had a characteristic time course, which was similar across images for a given neuron, but different across neurons. For example, consider the activity of three example neurons exhibiting a range of latencies, in response to three example images (**Figure 1**b). The amplitude of the responses differed across neurons: the first responded to images 1 and 2; the second to images 1 and 3, and the third to all three images. However, the time course of their responses seemed largely constant across images. The same results were obtained when looking at the responses to all images (**Figure 1**c): the delay of the responses showed a strong variation across neurons but a small variation within neurons (comparison of variance of delays across neurons vs. across images in this example session: $p < 0.001$, $n = 198$ neurons and $n = 112$ images, two-sided Wilcoxon rank sum test, **Figure 1**d,e).

The responses of each neuron across image stimuli could be well approximated as the product of a single time course and a single tuning profile. For each neuron, we applied non-negative matrix factorization to the matrix of responses as a function of time and image, and took the first component to obtain the best time course (one value at each time point) and the best tuning profile (one value for each image). The product of the two (a rank-1 approximation) provided a good summary of the original responses (**Figure 1**c,f). Indeed, cross-validation revealed that the rank-1 approximation was superior to models that used more terms in 87 ± 2 % of the recorded neurons across all 11 mice (**Figure 1**g,h).

The characteristic time courses of the neurons formed a graded sequence. We used the sorting algorithm Rastermap[34] to order the neurons in a sequence based on their time courses, with neurons firing early at the top and neurons firing late at the bottom. We obtained two such sequences, one for Wide Spiking neurons (WS), which are largely excitatory, and one for Narrow Spiking neurons (NS), which are presumed inhibitory[35]. This procedure revealed that the time courses of the recorded neurons cover a graded sequence (**Figure 1**i). The activity of both WS and NS neurons spanned the whole sequence.

This sequence proved to be a remarkably stable property of the neuronal population, remaining constant over weeks. Indeed, the sequence obtained on one day was essentially unchanged the next day (**Figure 1**i,j). This level of stability was observed over weeks, with minimal signs of change over 30 days of recordings (slope = -0.002 ± 0.001, mean ± s.e., n=4 mice**, Figure 1**k). In all 4 mice, the neurons' time courses were more stable than their tuning (slope = -0.006 ± 0.002, mean ± s.e., n = 4 mice), which showed a larger change over those 30 days (although not significant, $p = 0.11$, $n = 4$, paired t-test, **Figure 1**l). This change in tuning is consistent with reports of drifts in the visual representation[21,25] (but see Refs. [26-29]).

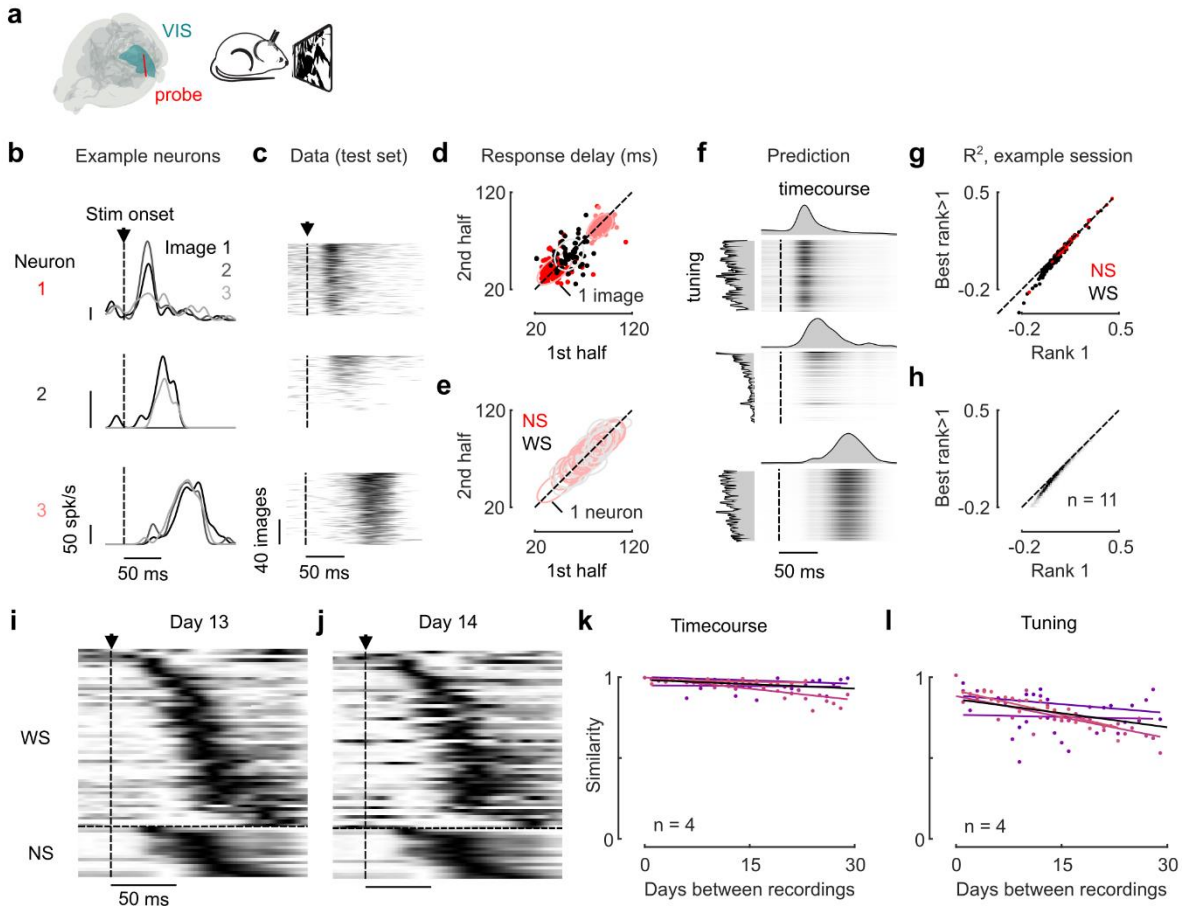

Figure 1. **Stimulus-evoked activity sequences in visual cortex are largely invariant to stimulus and stable across days**. **a**. Experimental setup for visual cortex (VIS) activity recordings and visual stimulation. **b**. Peri-stimulus histograms (PSTHs) of 3 example neurons in response to 3 example natural images (shades of grey). **c**. PSTHs of the same 3 neurons in response to all images. Images were ordered by decreasing response amplitude for each neuron, measured on one half of the data (train set), while we display the responses on the other half (test set). **d**. Response delay of each neuron to each image, for both halves of the data. Response delay was quantified as the centre of mass of the PSTHs. The ellipses show a fit of the distributions of the delays. **e**. Distribution of delays across all neurons. **f**. Prediction of the responses to all images on the test set for the same neurons as in **b** and **c**. The prediction comes from a "rank-1" model, which multiplies a single time course (top of each heatmap) with a single tuning profile (left of each heatmap). **g**. Quality of fit of a rank-1 model vs. the best model with a rank higher than 1 and up to 4 for all neurons within an example session. **h**. Same as **g**, for all neurons across all sessions of all animals. **i**. Time courses obtained from the rank-1 model for all neurons, sorted by Rastermap[34], for the example session (normalized by their peak). **j**. Same as **h**, but during the following day, after tracking the same neurons across both sessions. **k**. Similarity (noise-corrected correlation) of the neurons' time courses across recordings. **l**. Similarity of the neurons' tuning profiles across recordings.

We then asked whether we could find similar sequential structure in spontaneous activity. To do so, we considered the coupling of each individual neuron to the summed activity of all neurons (the population rate; **Figure 2**a,b). Specifically, we computed the spike-triggered population rate[8] for each neuron, which we refer to as "population coupling" (**Figure 2**c). The strength of this coupling at zero delay is a primary determinant of the pairwise correlations in a population[8] and (unlike correlation[36]) is not affected by the neuron's firing rate[8]. As expected[8], the strength of population coupling exhibited a large variation across neurons, with some neurons ("choristers") highly coupled to the population and others ("soloists") barely coupled (**Figure 2**c,e). In addition, we measured the delay of each neuron to population activity by computing the centre of mass of the population coupling profile; this is negative for "leader[10]" neurons which fire earlier than the majority of their neighbours, and positive for "follower[11]" neurons that fire after their neighbours. Neurons varied in both measures (**Figure 2**c), with no hint of relationship between the two: the correlation

between coupling strength and delay was 0.05 ± 0.05 in WS cells, and 0.06 ± 0.15 in NS cells (mean ± s.e., p = 0.64 for WS cells, p = 0.76 for NS cells, n = 11 mice, two-sided Wilcoxon test, **Figure 2**d). The two measures thus define largely independent axes to describe population structure.

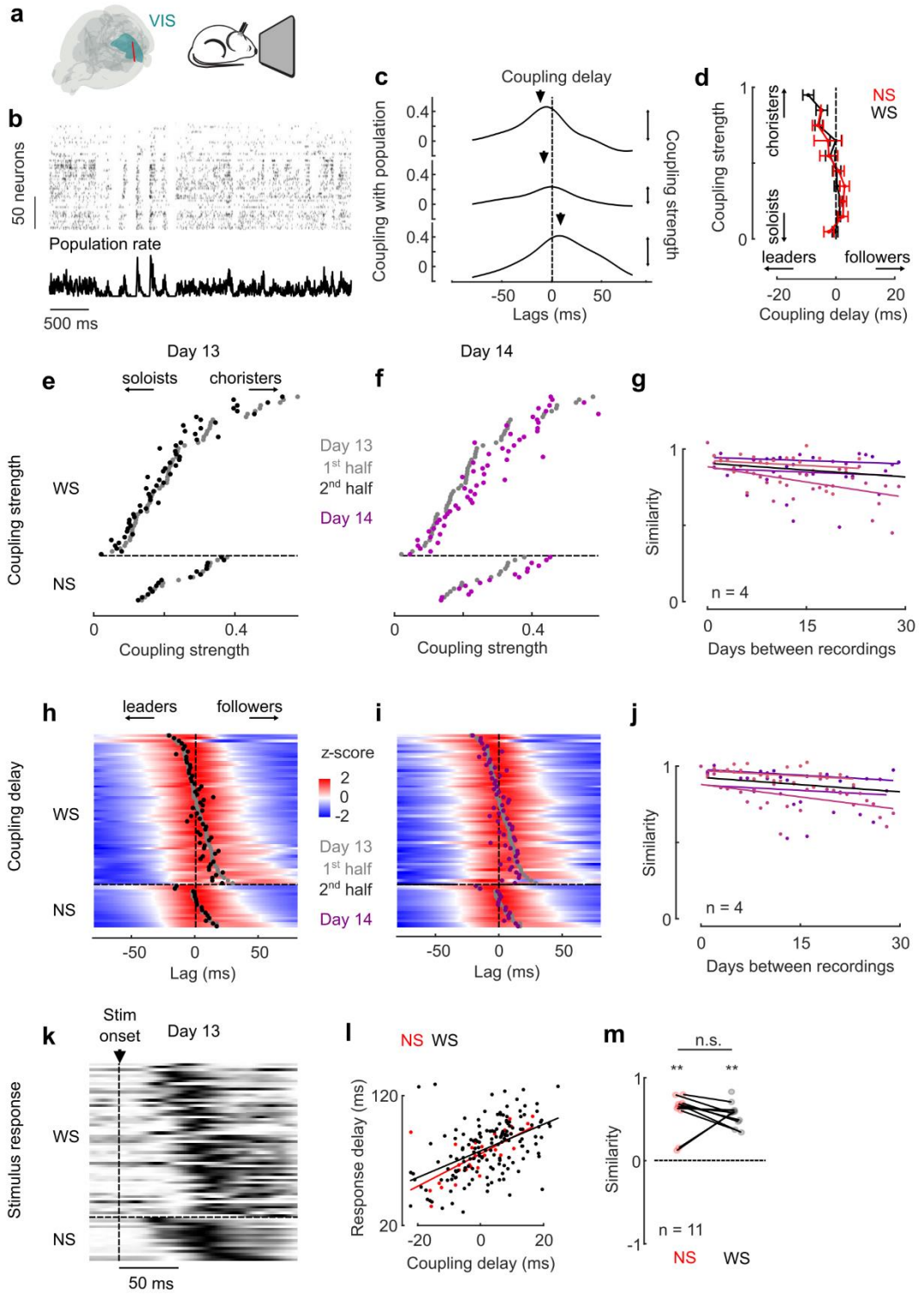

Figure 2. **Spontaneous activity sequences in visual cortex are stable across days and resemble evoked sequences. a**. Experimental setup for spontaneous activity recordings. **b**. Example raster of spontaneous activity (top) and average population rate (bottom). **c**. Coupling with the population for 3 example neurons. Two properties were extracted: the coupling strength, i.e. the value of the coupling at time 0, and the coupling delay, i.e. the centre of mass of the population coupling. **d**. Relationship between the coupling strength and the coupling delay of WS (*black*) and NS (*red*) neurons, averaged across all mice (n = 11, mean ± s.e.). **e**. Coupling strength

across all neurons for an example session recorded on day 13. Neurons were ordered by decreasing coupling strength and separated according to their spike waveform (WS: wide spiking; NS: narrow spiking). Within days, the coupling strength for each neuron was computed for both the 1st (*grey dots*) and the 2nd (*black dots*) halves, showing high reliability. **f**. Same as **e**, on the next day, after tracking the same neurons across recordings. A high reliability was also observed between the two days (*grey dots:* day 1, 1st half; *purple dots*: day 2, average over both halves). **g**. Similarity of the neurons' coupling strength across recordings. **h-j**. Same as **e-g**, but for coupling delays. Population couplings were z-scored for each neuron and ordered by their coupling delay during the 1st half of the session. **k**. Stimulus-evoked time courses of the same neurons, ordered as in **h** and **i** by delay during spontaneous sequences. **l**. Comparison of the spontaneous coupling delays and evoked responses delays, for both the putative excitatory (*black*, WS) and inhibitory (*red*, NS) neurons, in an example session. **m**. Similarity of the evoked and spontaneous delays across all animals (n = 11).

Thanks to the variation in coupling delay, the spontaneous activity in the mouse visual cortex thus formed stereotyped sequences (**Figure 2**h), similar to the sequences observed after eye movements and stimulus onsets[13,14] and to the spontaneous sequences observed in other cortical regions in other species[2,11,12,15,16].

Both the magnitude and delay of population coupling were highly consistent over weeks. A cell's coupling strength was largely constant across recording sessions (**Figure 2**f), exhibiting a similarity that showed little sign of decay across weeks (slope = -0.003 ± 0.001, mean ± s.e., n = 4 mice, **Figure 2**g): neurons that are choristers one day, remain so.

The sequences seen during spontaneous activity also remained stable over time. The spontaneous sequences measured on one day were essentially identical the next day (**Figure 2**h,i), with the coupling delay showing a similarity that showed little sign of decay over weeks (slope = -0.003 ± 0.001, mean ± s.e., n = 4 mice, **Figure 2**j).

Moreover, the sequences seen during spontaneous activity strongly resembled the sequences evoked by visual stimuli. To illustrate the similarity, we reordered the sequence we had seen in response to images (**Figure 1**i) so that neurons have the same ordering as the spontaneous sequences (**Figure 2**k). The spontaneous and driven sequences are clearly similar, and indeed the response delay correlated strongly with the coupling delay measured during spontaneous activity in this example session (r = 0.53) (**Figure 2**l). We computed the similarity of the two (Methods) and found it to be significant for both WS and NS neurons (WS: similarity s = 0.58 ± 0.18, p = 0.002; NS: s = 0.66 ± 0.18, p < 0.001, n = 11 mice; median ± mad, two-sided Wilcoxon signed-rank test), with no significant difference between the two (p = 0.43, paired two-sided Wilcoxon signed-rank test) (**Figure 2**m).

We next asked whether similar sequential patterns of activity occur also in other brain regions. We did so using acute recordings covering an entire hemisphere of the mouse brain, which we have performed with the International Brain Laboratory[37]. We examined the activity of 54,451 neurons in 229 brain regions, obtained from 416 recordings involving 640 insertions of Neuropixels 1.0 and 2.0 probes[32,38]. We further selected recordings with at least 5 neurons, selecting 240 brain regions. We focused on periods of spontaneous activity (recorded after the mice had performed the IBL task) and performed the same analysis that we had performed on the spontaneous activity of the primary visual cortex (**Figure 3**a). Because the electrophysiological signatures of different cell types are generally less understood outside the cortex, in these brainwide recordings we did not attempt to separate putative excitatory and inhibitory neurons.

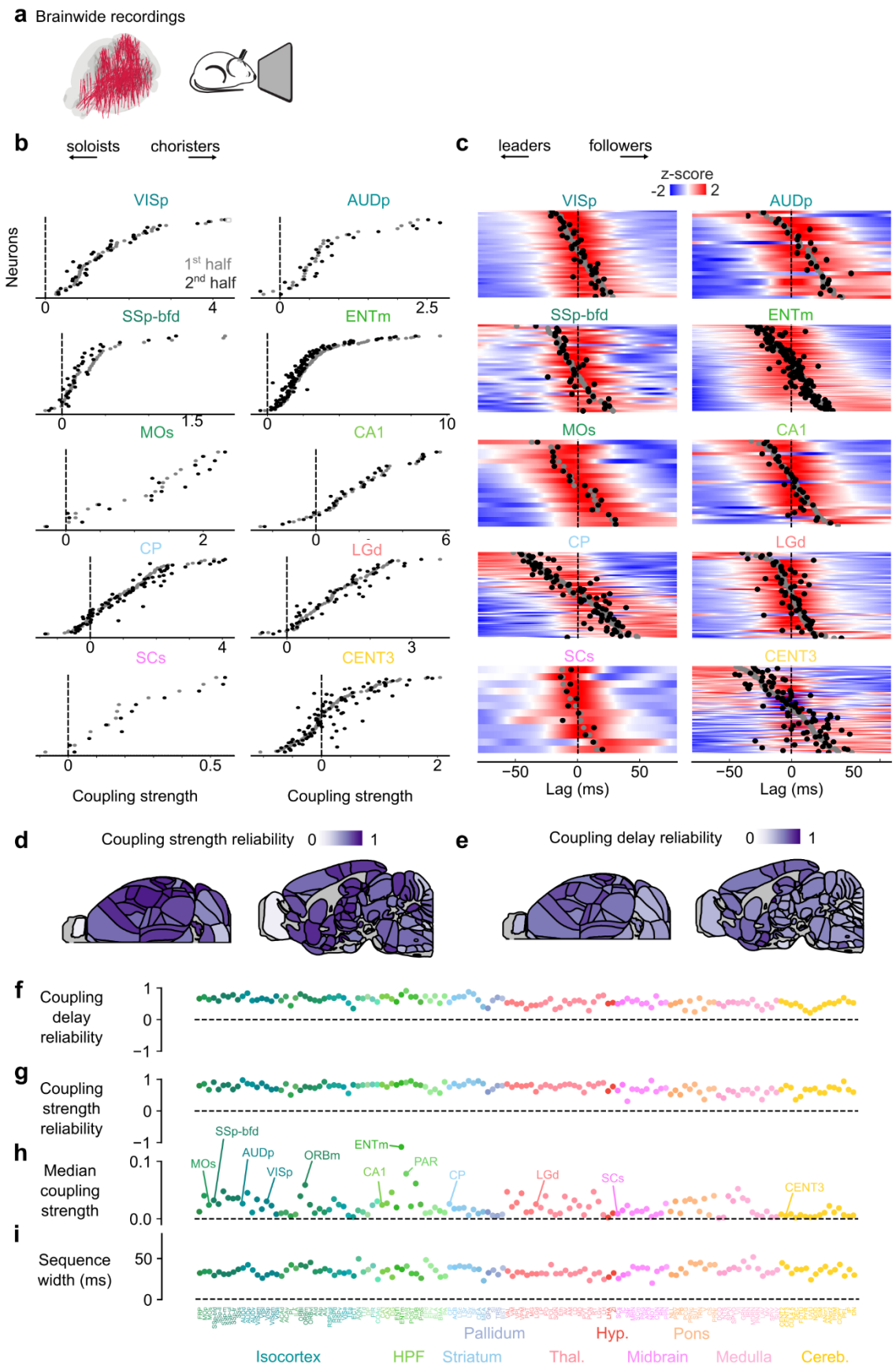

Figure 3. **Spontaneous activity sequences are found across the entire mouse brain. a**. Brainwide recordings from the International Brain Laboratory brainwide map dataset[37]. **b**, Population coupling strength across 10 example brain areas, cortical and subcortical: primary visual cortex (VISp), primary auditory cortex (AUDp), the barrel field in primary somatosensory area (SSp-bfd), medial

entorhinal cortex (ENTm), secondary motor area (MOs), hippocampal field CA1, caudate-putamen (CP), dorsal lateral geniculate nucleus (LGd), superficial superior colliculus (SCs), and central lobule III in the cerebellum (CENT3). The coupling strengths are shown for both the first (*grey*) and the second (*black*) half of each session. **c**. Z-scored population coupling for the same brain regions as in **b**, showing the coupling delays. **d**. Coupling strength reliability across the brain. **e**. Same as **d**, for the mean coupling delay reliability. **f**. Coupling delay reliability within days across all 137 recorded brain regions with at least 5 recordings. **g**. Same as **f**, with the mean coupling strength reliability within days. **h**. Same as **f**, with the median coupling strength. **i**. Same as **f**, with the sequences' width.

Sequences of activation appeared in essentially every brain region. For every brain region, we measured the strength and delay of the coupling of each neuron's activity to the population of neurons in the same region, assessing their reliability by correlating the measures obtained in two separate halves of a given recording. Neurons in essentially all brain regions showed reliable and diverse strengths of population coupling, with "soloist" neurons showing low coupling and "chorister" neurons showing strong coupling (**Figure 3**b). Furthermore, essentially all regions also contained reliable sequences of activation, with the activity of "leader" neurons preceding that of "follower" neurons (**Figure 3**c). As examples, we illustrate these results both in areas of the cerebral cortex where the sequences have already been observed, such as the primary visual[14], auditory[2] and somatosensory[2,12] (VISp, AUDp, SSp) areas and in additional regions such as prefrontal cortical area (MOs) and subcortical regions in hippocampal formation (ENTm and CA1), the striatum (CP), visual thalamus (LGd), superior colliculus (SCs) and cerebellum (CENT3).

To verify the robustness of these findings, we showed that coupling magnitude and delay were both highly reliable (consistent across two separate halves of a recording) in 137 out of the 137 brain regions (selected with at least 5 recordings, **Figure 3**d-g). Coupling magnitude, however, was uneven across brain regions. In some regions it was stronger than in the primary sensory areas: for instance, it appeared to be particularly strong in the parasubiculum (PAR), in the orbitofrontal cortex (ORB), and in the medial entorhinal cortex (ENTm) (**Figure 3**h). The duration of the sequences, by contrast, was fairly similar across regions: the range of coupling delays had an average of 35 ms and standard deviation of 6 ms across brain regions (n = 137, **Figure 3**i).

We finally asked whether the coupling and the sequences of activity that are observed across the brain are coordinated with each other. Though simultaneous recordings were not the goal of the IBL brainwide map, each Neuropixels probe invariably recorded from more than one region, and each session typically involved recordings from two probes. We can thus ask if the coupling that we have observed within all brain regions also occurs across regions. To illustrate the approach, consider a session where primary visual cortex (VISp) was recorded at the same time as medial entorhinal cortex (ENTm, **Figure 4**a,b). In this session, we can use the population activity in VISp as a "source" to measure population coupling not only in VISp itself (**Figure 4**c) but also in ENTm (**Figure 4**d), which are both "targets". The same analysis can be run by using ENTm as the source, and measuring the coupling to this source population in both target regions (**Figure 4**e,f).

The results of this analysis revealed that neuronal coupling extends beyond individual brain regions, with sequences of activation coupled across brain regions. For example, the activity in ENTm is coupled to the activity in VISp, and forms a sequence that is synchronous to the one occurring there (**Figure 4**d). Similarly, the activity in VISp is coupled to the activity in ENTm, and forms a sequence that is synchronous to the one occurring there (**Figure 4**e). The sequences in each target region, however, showed some reliable dependence on the source region (the sorting of neurons in **Figure 4**c,d is somewhat different from the one in **Figure 4**e,f), perhaps suggesting that the order of the sequence contains a signature of the region to which it is coupled.

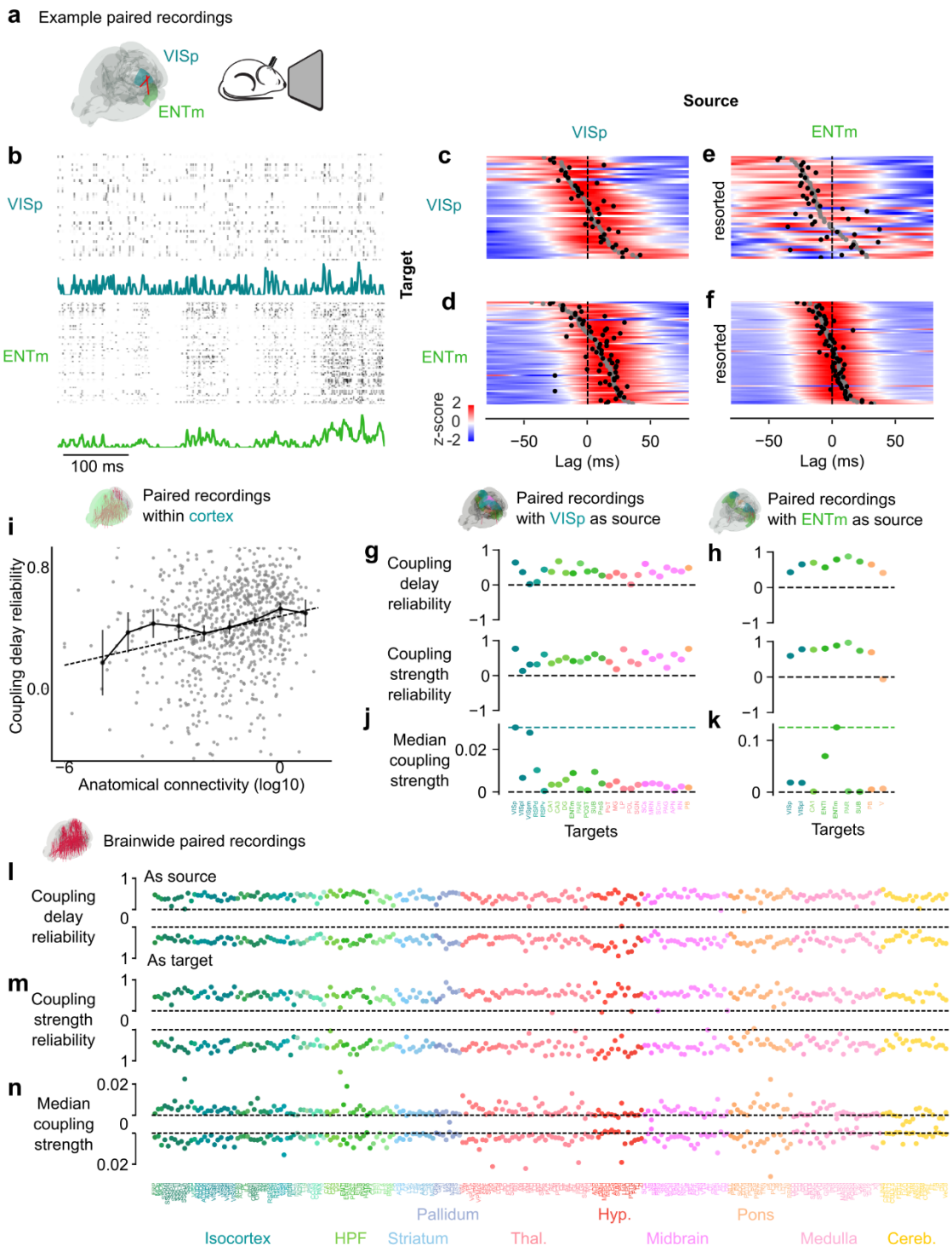

Figure 4. **Activity sequences are partly synchronized across brain areas. a**. Example paired recording. **b**. Rasters of activity with individual neurons activity in VISp (top) and ENTm (bottom), and VISP and ENTm average population rates. **c**. Z-scored coupling of VISp neurons with VISp population rate, with the coupling delays for the 1st half (*grey dots*) and the 2nd half (*black* dots) of the recordings. **d**. Same as **c**, with VISp as a source and ENTm as a target. **e**. Same as **c**, with ENTm as a source and VISp as a target. Neurons were resorted based on their coupling delay with ENTm. **f**. Same as **e**, with ENTm as a source and ENTm as a target. **g**. Coupling delay and coupling strength reliability of each brain region paired with VISp. **h**. Same as **g**, for each brain region paired with ENTm. **i**. Relationship between the coupling delay reliability of each pair of recording regions with their anatomical connectivity, measured by the Allen Institute Connectivity Atlas[39]. **j, k.** Same as **g, h**, with the median coupling strength. The dashed line shows the median coupling strength for VISp (**j**) and ENTm (**h**). **l-n**. Coupling delay reliability (**l**), coupling strength reliability (**m**) and median coupling strength (**n**) for each brain region as a source, averaged over all targets (top) or as a target, averaged over all sources (bottom).

We next measured the coupling of each source region with each of the target regions that were recorded simultaneously with it, and found a relation between coupling and anatomical connectivity. For example, 24 regions ("targets") were recorded simultaneously with VISp ("source", **Figure 4**g), and 8 regions were recorded simultaneously with ENTm (**Figure 4**h). For each of these combinations of targets and source, we computed the reliability of coupling strength and of coupling delay, and found them to be generally high: 24 out of 24 brain regions were reliably coupled to VISp, and 7 out of 8 to ENTm (**Figure 4**g**,**h). In the cerebral cortex, moreover, the coupling reliability was correlated with the anatomical connectivity measured by the Allen Institute Connectivity Atlas[39] (**Figure 4**i). The mean coupling strength, however, was generally much lower across regions than within a region (**Figure 4**j,k). This was true in 224 out of 240 brain regions as sources, and 217 out of 240 as targets.

Overall, each brain region exhibited reliable coupling with the rest of the regions that were recorded simultaneously with it, whether as a source or as a target. For each brain region (target), we computed the reliability of its coupling with all other simultaneously recorded regions (sources). We then obtained two averages: one over sources and one over targets. The former measures the overall coupling of neurons in each target region with the population rate of source regions, and the latter measures the overall coupling of the population rate of each source region to neurons outside it. Cross-area coupling delay and coupling strength were reliable in practically all regions (at least 237 out of 240), regardless of whether they were taken as a source or as a target (**Figure 4**l,m). The results show that practically all brain regions are effective sources and targets of coupling, with reliable strengths and sequence delays. The strengths of the coupling, however, showed some variation across regions (**Figure 4**n), and was invariably lower than the strength of coupling within regions (**Figure 3**h). Therefore, while the strongest coupling is seen within brain regions, coupling and the associated sequences are reliably present, synchronized, and distributed across the brain.

Discussion

Our results demonstrate that neural activity exhibits strong coupling and is organized in 50-100 ms sequences not only in some areas of the cerebral cortex but also in essentially every region of the mouse brain, displaying sequences that are coordinated not just within but also across regions. These findings in the mouse brain extend those previously been obtained in the mouse visual cortex[13,14], and in the somatosensory[2,12] and auditory[2] cortex of the rat. Given that sequences have also been observed in the cerebral cortex of reptiles[11,40] and primates[14], including humans[15,16], it is tempting to speculate that they might be ubiquitous, shaping the structure of brainwide activity in all vertebrates.

Claiming the existence of patterns in neural activity could be controversial if the claim is based on complex and potentially biased statistical measures. To ensure robustness and transparency we adopted extremely simple statistical measures: for each neuron we computed the population coupling[8] (which is simply the spike-triggered population rate) and we measured its height at delay zero (yielding coupling strength) and its centre of mass (yielding coupling delay)[12], assessing reliability by cross-validation: dividing the data in two within a session (or where applicable across sessions), and correlating the results across the two halves.

The sequences that we have observed across the brain interacted multiplicatively with the firing rate code, constraining but not mandating or impeding the participation of individual neurons. Indeed, in the visual cortex the participation of individual neurons in an activity sequence elicited by an image depended on the tuning of those neurons to that image. However, if the tuning of the neurons is such that they respond to the image, then their response occurred at a specific time in the sequence, which was largely fixed for each neuron. More precisely, the sequences interacted multiplicatively with the firing rate code that

describes the tuning of the neurons, so that at any given time and for any given image, the response of the neuron was the product of a tuning curve that depends on images but not time, and a response profile that depends on time but not on images.

By recording from the same neurons in visual cortex over time, we established that the sequences are stable over weeks. In our 4 chronically recorded animals, the sequences were more stable than the representation of visual stimuli, which (consistent with some[20-24] but not all[26-31] reports) showed some apparent drift. This stability agrees with the view that the sequences constitute a hard-wired scaffold[16] for neural activity. However, it is also possible that dynamical processes may in some cases modify the sequences through learning or plasticity[13].

As had been seen in other cortical areas in rats[2,12] and humans[15,16], the sequences occurred not only during sensory-driven activity but also during spontaneous activity. The fact that both forms of activity are constrained to the same spatiotemporal patterns might help explain the similarity between spontaneous and driven activity that has been reported multiple times (e.g. Refs. [1,2,41-44]). The occurrence of the sequences during spontaneous activity was also a welcome observation in that it allowed us to extend the analysis from a region where we could elicit activity at will – the visual cortex – to the rest of the brain, where activity is generally ongoing and less easily elicited.

The sequences we have observed across the brain were very similar to the 50-100 ms sequences measured in various cortical regions[2,11-16,40], but their duration was on the short end: the median sequence duration averaged ~35 ms across regions. It is hard to know if this duration is significantly shorter than in previous studies, however, because those studies did not quantify the sequence duration.

These rapid sequences may bear some relation to the sequences observed in hippocampal "replay[45-48]" and "preplay[49-51]", which typically last hundreds of milliseconds. These longer sequences appear not only in hippocampus but also in visual[48] and prefrontal cortex[52], so, just as with the rapid sequences studied here, they may also appear in other brain regions. Though the rapid sequences are much briefer than the "preplay" and "replay" patterns, they are on the same time scale as the theta cycle, and as such they may be related to the alternating "sweeps" observed in hippocampus and entorhinal cortex during the theta cycle and during REM sleep[53].

The rapid sequences we observed also appear to differ from other sequences observed in various neural systems, which are generally substantially longer. These include 0.5-1.0 s songs in the zebra finch's premotor nucleus HVC[54]; ~1 s sequences in ex vivo slices of mouse cortex[55]; ~1.5 s "playback" patterns in prefrontal cortex[56]; multi-second sequences in many brain regions[57] associated with arousal events[58]; periodic multi-second sequences in medial entorhinal cortex[59]; and multi-second sequences in the mouse visual cortex[60].

The circuit basis of the sequences is currently unknown, but may arise from simple and known factors. Sequences of various durations arise readily in silico[40,61] and even in organoids[62]. Suggested mechanisms generally involve a synaptic chain of activation[40] shaped by intrinsic excitability[63] and conduction delays[64].

The ubiquity of sequences suggests that they underlie a canonical computation operating across the brain. Sequences of spiking activity have been suggested as potential building blocks of information[10], controlling the precision of sensory processing[14] or creating sequences of motor actions[63]. Moreover, the synchronicity of the sequences across pairs of regions suggests that sequences of activity may be triggered throughout the whole brain simultaneously. Moreover, different sequences may be associated with different source regions, generating a specific temporal "fingerprint" within each target region. The functional role of brainwide sequences, however, remains unknown. Addressing these questions will likely require new datasets obtained with massively parallel brainwide recordings.

Acknowledgements

We would like to thank Anna Lebedeva, Michael Okun, Enny van Beest, and Agnès Landemard for their help with various aspects of the data and analysis, and Amirreza Bahramani for his comments on the manuscript. This research was funded by the Wellcome Trust (Investigator Award 223144/Z/21/Z to MC and KDH, and Early Career Award 227065 to CB). MC holds the GlaxoSmithKline / Fight for Sight Chair in Visual Neuroscience.

Author contributions

Conceptualization, funding acquisition, resources, and writing—review and editing: C.B., K.D.H. and M.C.; Methodology, software, formal analysis, and investigation: C.B.; Visualization and writing—original draft: C.B. and M.C.; Supervision: M.C.

Data availability

Part of the data is already available online[32] (https://doi.org/10.5522/04/24411841), and the rest will be made available upon publication.

Code availability

The code will be made available upon publication.

Methods

Our study is based on two main datasets: one involving chronic recordings in the mouse visual cortex, performed in our laboratory, and one involving acute brainwide recordings, performed in collaboration with the International Brain Laboratory[37].

Chronic recordings in visual cortex

Experimental procedures at UCL were conducted according to the UK Animals Scientific Procedures Act (1986) and under personal and project licenses released by the Home Office following appropriate ethics review.

Surgeries

A brief (~1 h) initial surgery was performed under isoflurane (1–3% in O_2) anaesthesia to implant a headplate made of titanium (~25 × 3 × 0.5 mm, 0.2 g) or steel (~25 × 5 × 1 mm, 0.5 g). In brief, the dorsal surface of the skull was cleared of skin and periosteum. A thin layer of cyanoacrylate was applied to the skull and allowed to dry. Thin layers of ultraviolet (UV)-curing optical glue (Norland Optical Adhesives #81, Norland Products) were applied and cured until the exposed skull was covered. The head plate was attached to the skull over the interparietal bone with Super-Bond polymer. After recovery, mice were treated with carprofen or meloxicam for 3 days, then acclimated to handling and head fixation.

Mice were then implanted with chronic Neuropixels 2.0 probes using one of 4 possible implants (see section 'Implants' below). Briefly, implantation was performed under isoflurane (1–3% in O_2) anaesthesia and after injection of Colvasone and Rimadyl. The UV glue was removed, and the skull was cleaned and scarred for best adhesion of the cement. The skull was levelled, and a craniotomy was performed using a drill or a biopsy punch. Once exposed, the brain was covered with Dura-Gel (Cambridge Neurotech). Probes were implanted in left or right primary visual cortex (2.5 mm lateral, 3.5 mm posterior from Bregma, one probe per animal).

Implants

For the implants, we used multiple strategies: in 4 mice we used a cemented implant[32] and in 7 mice we used a recoverable modular implant[32,33,65,66]. The choice of implant did not affect the results.

Cemented implant. Mice were implanted by holding and inserting the probes using a cemented dovetail and applying dental cement to encase the probe printed circuit board and reliably attach it to the skull. The recordings were made in external reference mode, using the silver wire or the headplate as the reference signal. The data from these four mice were already published[32].

Recoverable modular implants. Mice were implanted recoverable, modular implants, such as the "Apollo" implant[33] (3 mice) , the 'Haesler' implant[65] (1 mouse), or the 'Repix' implant[66] (3 mice). The methods for each implant are described in their respective papers. Briefly, after carefully

positioning of the shanks at the surface of the brain, avoiding blood vessels, probes were inserted at slow speed (3–5 µm/s). Before surgery, the probes were coated with fluorescent dye DiI (ThermoFisher) by either manually brushing each probe with a droplet of DiI or dipping them in directly in DiI, for histological reconstruction. Once the desired depth was reached (optimally, just before the docking module touched the skull), the implant was sealed using UV glue, then covered with Super-Bond polymer, ensuring that only the docking module was cemented. After finishing all recording sessions, the probes were explanted and cleaned before reusing. The recordings were made in external or internal reference mode, using the headplate as the reference signal.

Anatomical reconstruction

We imaged the brains using serial section[67] two-photon[68] tomography. Our microscope was controlled by ScanImage Basic (Vidrio Technologies) using BakingTray[69] (github.com/SWC-Advanced-Microscopy/BakingTray). Images were assembled using StitchIt[70] (github.com/SWC-Advanced-Microscopy/StitchIt). Brains were aligned to the Allen Brain Atlas [71] and probe location was checked using brainreg[72] or through custom software (www.github.com/petersaj/AP_histology). This showed that most recordings were in area VISp, and partially in high-visual areas. The exact location of the probe in visual cortex did not affect the results so we pooled all visual areas together under the name of visual cortex (VIS).

Data acquisition and processing

Data were acquired using SpikeGLX (billkarsh.github.io/SpikeGLX/), and each session was spike-sorted with Kilosort2.5[32]. Well-isolated units were selected using Bombcell[73] (github.com/Julie-Fabre/bombcell; using parameters defined in bc_qualityParamValuesForUnitMatch.m). To track neurons across days, we used UnitMatch[18], which uses the waveform of individual neurons within each recording to compute a pairwise probability of matching across all pairs. We used the "intermediate" level of conservativeness to determine whether units were tracked across days. Neurons were categorized as "Narrow Spiking" if their waveform duration was lower than 0.4 ms, and "Wide Spiking" otherwise.

Stimuli

In each session, mice were presented with 112 natural images, repeated 5 times in a random order and separated by a static grey screen. The images were local contrast-normalized and were the same as in Ref. [32]. Depending on the protocol, images were presented for 1s with fixed 2s inter-trial intervals, or for 0.5s with fixed 0.8s inter-trial intervals. "Spontaneous" periods were defined as all time-periods without a stimulus on the screen, excluding a 0.3s window after the offset of each stimulus. Visual stimuli were presented through three displays (Adafruit, LP097QX1), each with a resolution of 1024 × 768 pixels. The screens covered approximately 270 × 70 degrees of visual angle, with 0 degrees being directly in front of the mouse, and images were presented on the front and contralateral screens. The screens had a refresh rate of 60 frames per second and were fitted with Fresnel lenses (Wuxi Bohai Optics, BHPA220-2-5) to ensure approximately equal luminance across viewing angles.

IBL dataset

We used Neuropixels recordings in the mouse brain performed in our consortium of laboratories as detailed elsewhere[37] (revision: 2024-05-06). Specifically, we focused on 416 sessions that contained a period of spontaneous activity, where the screen was grey. These recordings, using 640 probes, spanned 229 regions, totalling 54,451 neurons.

Data analysis

Stimulus-evoked activity

PSTHs. To compute the peri-stimulus time histograms (PSTHs), we computed for each neuron the number of spikes within 1ms time bins ranging from 25 ms before to 150 ms after the stimulus onset. We then temporally smoothed the PSTHs with a 30 ms-wide gaussian window (σ = 5.8 ms).

NMF model. To explain the response of single neurons across images, we performed Non-

negative Matrix Factorization (NMF) on the response matrix of individual neurons R of elements $R_{t,i}$ (number of time points x number of images) using a range of factors from 0 to 4 which defined the rank of our prediction:

$$R = WT$$

where W contains the tuning components (size number of factors x number of images) and T the temporal components (size number of timepoints x number of factors). For example, the rank-0 model consisted simply in a uniform firing rate, the rank-1 model consisted in a single time course multiplied with a single tuning profile, and more generally the rank-n model contains n time courses associated with n tuning profiles. To measure the goodness of the model, we computed the coefficient of determination R^2 between the prediction and the test set. To compute the R^2 across models (**Figure 1**g,h), we used a leave-one-out cross-validation procedure where four repeats were used for training and one for testing. In **Figure 1**c,f, we used half of the repeats to plot the neurons' response, and the other half to compute the model.

Population coupling

We performed the same analyses on both datasets.

Spike-triggered population rate. To measure population coupling, we first binned the firing rate of neurons in 1ms time bins, focusing on spontaneous periods, obtaining the raw firing $f_i(t)$ of neuron i across time. We then computed the spike-triggered population rate (stPR, $c_{i,\tau}$), similarly to Ref. [8] and defined as:

$$c_{i,\tau} = 100 * \frac{1}{\|f_i\|} \int f_i(t - \tau) \frac{1}{N-1} \sum_{j \neq i} \left(f_j(t) - \mu_j\right) dt$$

where τ represents the time lag between the neuron and the population, μ_i the average firing rate of neuron i, $\|f_i\|$ the number of spikes it fired, and N the total number of neurons in the recording. Note that compared to Ref. [8], we normalized by the number of neurons, time-lagged the analysis, and multiplied it by 100 to define it as a percentage. Importantly, the population coupling is uncorrelated with the neuron's firing rate[8].

To focus on 50-100 ms long sequences of activity, we computed coupling within a [-80 80] ms window, and low-passed filtered the coupling with a 20 Hz cutoff.

Coupling strength. The strength of the population coupling was defined at lag 0 ($c_{i,0}$). To summarize the overall level of coupling strength for each recording and brain area, we computed the median population coupling strength across all neurons within that brain area (**Figure 3**h, **Figure 4**j,k,n).

Sequences

We generally defined a neuron's delay by computing its centre of mass d, defined as follows:

$$d = \frac{\sum_{t=t_1}^{t_2} F_t * t}{\sum_{t=t_1}^{t_2} F_t}$$

Where F_t if the normalized metric (firing rate, population coupling) at time t, within the time window $[t_1, t_2]$.

Stimulus-evoked sequences. To compute each neuron's delay in response to individual images, we measured the centre of mass of the PSTH averaged over the repeats of that image within a "responsive window". The "responsive window" was defined as the timepoints within 20 to 150ms after stimulus onset where the firing rate of the neuron was at least two standard-deviations above its baseline. When no timepoints were filling this criterion, the centre of mass was set to *nan*. In **Figure 1**d,e, we fitted an ellipse to the distributions of delays for each neuron across the two halves and all images.

Similarly, to compute each neuron's average delay across all images, we performed a similar analysis on the time course component given by the rank-1 model.

Coupling delay. To compute each neuron's delay during spontaneous activity, we computed the centre of mass of their low-passed stPR. To visualize the sequences, we plotted a heatmap of

the stPR averaged across repeats, and displayed the coupling delays for both the first and the second half of the recording, sorted by the first half.

Sequence width. The sequence's width was defined as the difference between the 25th and the 75th percentiles of the coupling delays across neurons.

Reliability, similarity and stability

Reliability. To measure the reliability of the various metrics (coupling strength, delay, etc.), we split all recordings in two halves and performed the analysis on both halves. For stimulus-evoked responses, we used odd and even repeats of the same stimuli as the two halves. For population coupling strength or delay, we artificially cut the recording halfway. We then defined reliability as the correlation of the metric across the two halves.

Similarity. To measure the similarity s of metrics x and y across conditions (e.g. across stimulus condition, across days), we used noise-corrected correlation[74]. In short, noise-corrected correlation normalizes the z-transformed average correlation of the metric across conditions by the reliability of the metric within condition:

$$s(x,y) = \frac{\text{z-mean}(\rho(x_1,y_2),\rho(x_2,y_1))}{\sqrt{\rho(x_1,x_2)\,\rho(y_1,y_2)}}$$

where ρ denotes the Pearson correlation coefficient, and x_1, x_2 and y_1, y_2 are the vectors of metric x and y for the two halves of the data. The function z-mean computes the average of the z-transformed correlation coefficient before inverse z-transforming it:

$$\text{z-mean}(\rho_1,\rho_2) = \text{atanh}(0.5 * \tanh(\rho_1) + 0.5 * \tanh(\rho_2))$$

To measure the similarity between evoked and spontaneous sequences, we used recordings where at least 10 neurons of each type were present. We computed the similarity of the centres of mass of the spontaneous population couplings and the centres of mass of the time course given by the rank 1 model.

Stability. To measure the stability of a metric across days, we simply computed the similarity of the metric across pairs of recordings. We selected pairs of recordings where at least 15 neurons were tracked, and selected animals with at least 5 recordings, with at least one pair of recordings more than 15 days apart, yielding 4 animals. To measure the stability of evoked responses (time course and tuning), we focused on neurons that were visually responsive, as defined by being better predicted by a model with a rank > 0 rather than its average firing rate, as defined by its cross-validated R^2.

The stability was then estimated performing a robust regression using the bisquare weighting function (*fitlm* in Matlab, with option 'RobustOpts' on). The average of the intercept and slope across mice was then used to show the average fit.

Cross-area analysis

Cross-area coupling. To compute cross-area coupling, we simply computed the time-lagged coupling of each neuron from one area (the 'target' area) with the average population rate of the other area (the 'source' area). We then computed the coupling strength and delay of each neuron of the target area relative to the source area.

We then obtained, for each metric of interest, a matrix of size (number of areas x number of areas) that was sparsely populated, depending on the available paired recordings. We then defined for each metric two summary statistics for each brain area: the average metric as a source (averaging over targets, excluding the area itself) and the average metric as a target (averaging over sources, excluding the area itself).

Connectivity and distance. We related the cross-area sequences to two anatomical metrics: axonal connectivity (axonal projection tracing[39]) and cartesian distance (inverse Euclidean distance between centroids of region pairs). To compute the connectivity between brain areas, we directly loaded the 41586_2014_BFnature13186_MOESM70_ESM.csv from Ref. [39] and extracted the quantitative projection signals for each pair of areas. To

compute the Euclidean distance between brain areas, we used the inverse distance between the centroids of each area, as in Ref. [37].

Inclusion criteria for the IBL dataset

To obtain the average values for each metric and each brain area across the IBL dataset, we selected recordings with at least 5 neurons in each area of interest. For example, for cross-area analysis, we would focus on paired areas where at least 5 neurons were recorded in both areas.

For within-area coupling (**Figure 3**), we further selected areas with at least 5 recordings. For cross-area coupling, we selected pairs of areas with at least 2 recordings for **Figure 4**f,g,j,k but took all pairs for for **Figure 4**l-m. This was because our conclusions do not focus on particular pairs of regions, but on the global reliability of coupling strengths and delays across the brain.

References

1 Ringach, D. L. Spontaneous and driven cortical activity: implications for computation. *Current Opinion in Neurobiology* **19**, 439-444 (2009). https://doi.org/10.1016/j.conb.2009.07.005

2 Luczak, A., Bartho, P. & Harris, K. D. Spontaneous events outline the realm of possible sensory responses in neocortical populations. *Neuron* **62**, 413-425 (2009). https://doi.org/10.1016/j.neuron.2009.03.014

3 Gallego, J. A., Perich, M. G., Miller, L. E. & Solla, S. A. Neural Manifolds for the Control of Movement. *Neuron* **94**, 978-984 (2017). https://doi.org/10.1016/j.neuron.2017.05.025

4 Gao, P. & Ganguli, S. On simplicity and complexity in the brave new world of large-scale neuroscience. *Current Opinion in Neurobiology* **32**, 148-155 (2015). https://doi.org/10.1016/j.conb.2015.04.003

5 Cunningham, J. P. & Yu, B. M. Dimensionality reduction for large-scale neural recordings. *Nat Neurosci* **17**, 1500-1509 (2014). https://doi.org/10.1038/nn.3776

6 Sadtler, P. T. *et al.* Neural constraints on learning. *Nature* **512**, 423-426 (2014). https://doi.org/10.1038/nature13665

7 Schneidman, E., Berry, M. J., 2nd, Segev, R. & Bialek, W. Weak pairwise correlations imply strongly correlated network states in a neural population. *Nature* **440**, 1007-1012 (2006).

8 Okun, M. *et al.* Diverse coupling of neurons to populations in sensory cortex. *Nature* **521**, 511-515 (2015). https://doi.org/10.1038/nature14273

9 Okun, M. *et al.* Population rate dynamics and multineuron firing patterns in sensory cortex. *J Neurosci* **32**, 17108-17119 (2012). https://doi.org/10.1523/JNEUROSCI.1831-12.2012

10 Luczak, A., McNaughton, B. L. & Harris, K. D. Packet-based communication in the cortex. *Nat Rev Neurosci* **16**, 745-755 (2015). https://doi.org/https://doi.org/10.1038/nrn4026

11 Hemberger, M., Shein-Idelson, M., Pammer, L. & Laurent, G. Reliable Sequential Activation of Neural Assemblies by Single Pyramidal Cells in a Three-Layered Cortex. *Neuron* **104**, 353-369 e355 (2019). https://doi.org/10.1016/j.neuron.2019.07.017

12 Luczak, A., Bartho, P., Marguet, S. L., Buzsaki, G. & Harris, K. D. Sequential structure of neocortical spontaneous activity in vivo. *Proc Natl Acad Sci U S A* **104**, 347-352 (2007). https://doi.org/10.1073/pnas.0605643104

13 Xu, S., Jiang, W., Poo, M. M. & Dan, Y. Activity recall in a visual cortical ensemble. *Nat Neurosci* **15**, 449-455, S441-442 (2012). https://doi.org/10.1038/nn.3036

14 Parker, P. R. L. *et al.* A dynamic sequence of visual processing initiated by gaze shifts. *Nat Neurosci* **26**, 2192-2202 (2023). https://doi.org/10.1038/s41593-023-01481-7

15 Vaz, A. P., Wittig, J. H., Jr., Inati, S. K. & Zaghloul, K. A. Replay of cortical spiking sequences during human memory retrieval. *Science* **367**, 1131-1134 (2020). https://doi.org/10.1126/science.aba0672

16 Vaz, A. P., Wittig, J. H., Jr., Inati, S. K. & Zaghloul, K. A. Backbone spiking sequence as a basis for preplay, replay, and default states in human cortex. *Nat Commun* **14**, 4723 (2023). https://doi.org/10.1038/s41467-023-40440-5

17 Dhawale, A. K. *et al.* Automated long-term recording and analysis of neural activity in behaving animals. *eLife* **6** (2017). https://doi.org/10.7554/eLife.27702

18 van Beest, E. H. *et al.* Tracking neurons across days with high-density probes. *Nat Methods* **22**, 778-787 (2024). https://doi.org/10.1038/s41592-024-02440-1

19 Lütcke, H., Margolis, D. J. & Helmchen, F. Steady or changing? Long-term monitoring of neuronal population activity. *Trends Neurosci* **36**, 375-384 (2013). https://doi.org/10.1016/j.tins.2013.03.008

20 Driscoll, L. N., Pettit, N. L., Minderer, M., Chettih, S. N. & Harvey, C. D. Dynamic Reorganization of Neuronal Activity Patterns in Parietal Cortex. *Cell* **170**, 986-999 e916 (2017). https://doi.org/10.1016/j.cell.2017.07.021

21 Marks, T. D. & Goard, M. J. Stimulus-dependent representational drift in primary visual cortex. *Nat Commun* **12**, 5169 (2021). https://doi.org/10.1038/s41467-021-25436-3

22 Schoonover, C. E., Ohashi, S. N., Axel, R. & Fink, A. J. P. Representational drift in primary olfactory cortex. *Nature* **594**, 541-546 (2021). https://doi.org/10.1038/s41586-021-03628-7

23 Aschauer, D. F. *et al.* Learning-induced biases in the ongoing dynamics of sensory representations predict stimulus generalization. *Cell Rep* **38**, 110340 (2022). https://doi.org/10.1016/j.celrep.2022.110340

24 Wang, H. C., LeMessurier, A. M. & Feldman, D. E. Tuning instability of non-columnar neurons in the salt-and-pepper whisker map in somatosensory cortex. *Nat Commun* **13**, 6611 (2022). https://doi.org/10.1038/s41467-022-34261-1

25 Bauer, J. *et al.* Sensory experience steers representational drift in mouse visual cortex. *Nat Commun* **15**, 9153 (2024). https://doi.org/10.1038/s41467-024-53326-x

26 Bondar, I. V., Leopold, D. A., Richmond, B. J., Victor, J. D. & Logothetis, N. K. Long-term stability of visual pattern selective responses of monkey temporal lobe neurons. *PLoS One* **4**, e8222 (2009). https://doi.org/10.1371/journal.pone.0008222

27 Tolias, A. S. *et al.* Recording chronically from the same neurons in awake, behaving primates. *J Neurophysiol* **98**, 3780-3790 (2007). https://doi.org/10.1152/jn.00260.2007

28 McMahon, D. B., Jones, A. P., Bondar, I. V. & Leopold, D. A. Face-selective neurons maintain consistent visual responses across months. *Proc Natl Acad Sci U S A* **111**, 8251-8256 (2014). https://doi.org/10.1073/pnas.1318331111

29 Sadeh, S. & Clopath, C. Contribution of behavioural variability to representational drift. *eLife* **11** (2022). https://doi.org/10.7554/eLife.77907

30 Jensen, K. T., Kadmon Harpaz, N., Dhawale, A. K., Wolff, S. B. E. & Olveczky, B. P. Long-term stability of single neuron activity in the motor system. *Nat Neurosci* **25**, 1664-1674 (2022). https://doi.org/10.1038/s41593-022-01194-3

31 Zhang, M. *et al.* The representation of decision variables in orbitofrontal cortex is longitudinally stable. *Cell Rep* **43**, 114772 (2024). https://doi.org/10.1016/j.celrep.2024.114772

32 Steinmetz, N. A. *et al.* Neuropixels 2.0: A miniaturized high-density probe for stable, long-term brain recordings. *Science* **372** (2021). https://doi.org/10.1126/science.abf4588

33 Bimbard, C. *et al.* An adaptable, reusable, and light implant for chronic Neuropixels probes. *eLife* (2025). https://doi.org/https://doi.org/10.7554/eLife.98522.2.sa4

34 Stringer, C. *et al.* Rastermap: a discovery method for neural population recordings. *Nat Neurosci* **28**, 201-212 (2025). https://doi.org/10.1038/s41593-024-01783-4

35 Bartho, P. *et al.* Characterization of neocortical principal cells and interneurons by network interactions and extracellular features. *J Neurophysiol* **92**, 600-608 (2004). https://doi.org/10.1152/jn.01170.2003

36 de la Rocha, J., Doiron, B., Shea-Brown, E., Josic, K. & Reyes, A. Correlation between neural spike trains increases with firing rate. *Nature* **448**, 802-806 (2007). https://doi.org/10.1038/nature06028

37 International Brain Laboratory *et al.* A brain-wide map of neural activity during complex behaviour. *Nature* **645**, 177-191 (2025). https://doi.org/10.1038/s41586-025-09235-0

38 Jun, J. J. *et al.* Fully integrated silicon probes for high-density recording of neural activity. *Nature* **551**, 232-236 (2017). https://doi.org/10.1038/nature24636

39 Oh, S. W. *et al.* A mesoscale connectome of the mouse brain. *Nature* **508**, 207-214 (2014). https://doi.org/10.1038/nature13186

40 Riquelme, J. L., Hemberger, M., Laurent, G. & Gjorgjieva, J. Single spikes drive sequential propagation and routing of activity in a cortical network. *eLife* **12** (2023). https://doi.org/10.7554/eLife.79928

41 Kenet, T., Bibitchkov, D., Tsodyks, M., Grinvald, A. & Arieli, A. Spontaneously emerging cortical representations of visual attributes. *Nature* **425**, 954-956 (2003). https://doi.org/10.1038/nature02078

42 MacLean, J. N., Watson, B. O., Aaron, G. B. & Yuste, R. Internal dynamics determine the cortical response to thalamic stimulation. *Neuron* **48**, 811-823 (2005).

43 Han, F., Caporale, N. & Dan, Y. Reverberation of recent visual experience in spontaneous cortical waves. *Neuron* **60**, 321-327 (2008). https://doi.org/10.1016/j.neuron.2008.08.026

44 Hoffman, K. L. & McNaughton, B. L. Coordinated reactivation of distributed memory traces in primate neocortex. *Science* **297**, 2070-2073 (2002). https://doi.org/10.1126/science.1073538

45 Skaggs, W. E. & McNaughton, B. L. Replay of neuronal firing sequences in rat hippocampus during sleep following spatial experience. *Science* **271**, 1870-1873 (1996).

46 Lee, A. K. & Wilson, M. A. Memory of sequential experience in the hippocampus during slow wave sleep. *Neuron* **36**, 1183-1194 (2002). https://doi.org/10.1016/s0896-6273(02)01096-6

47 Carr, M. F., Jadhav, S. P. & Frank, L. M. Hippocampal replay in the awake state: a potential substrate for memory consolidation and retrieval. *Nat Neurosci* **14**, 147-153 (2011). https://doi.org/10.1038/nn.2732

48 Ji, D. & Wilson, M. A. Coordinated memory replay in the visual cortex and hippocampus during sleep. *Nat Neurosci* **10**, 100-107 (2007). https://doi.org/10.1038/nn1825

49 Diba, K. & Buzsaki, G. Forward and reverse hippocampal place-cell sequences during ripples. *Nat Neurosci* **10**, 1241-1242 (2007). https://doi.org/10.1038/nn1961

50 Dragoi, G. & Tonegawa, S. Preplay of future place cell sequences by hippocampal cellular assemblies. *Nature* **469**, 397-401 (2011). https://doi.org/10.1038/nature09633

51 Farooq, U., Sibille, J., Liu, K. & Dragoi, G. Strengthened Temporal Coordination within Pre-existing Sequential Cell Assemblies Supports Trajectory Replay. *Neuron* **103**, 719-733 e717 (2019). https://doi.org/10.1016/j.neuron.2019.05.040

52 Shin, J. D., Tang, W. & Jadhav, S. P. Dynamics of Awake Hippocampal-Prefrontal Replay for Spatial Learning and Memory-Guided Decision Making. *Neuron* **104**, 1110-1125 e1117 (2019). https://doi.org/10.1016/j.neuron.2019.09.012

53 Vollan, A. Z., Gardner, R. J., Moser, M. B. & Moser, E. I. Left-right-alternating theta sweeps in entorhinal-hippocampal maps of space. *Nature* **639**, 995-1005 (2025). https://doi.org/10.1038/s41586-024-08527-1

54 Hahnloser, R. H., Kozhevnikov, A. A. & Fee, M. S. An ultra-sparse code underlies the generation of neural sequences in a songbird. *Nature* **419**, 65-70 (2002). https://doi.org/10.1038/nature00974

55 Dechery, J. B. & MacLean, J. N. Emergent cortical circuit dynamics contain dense, interwoven ensembles of spike sequences. *J Neurophysiol* **118**, 1914-1925 (2017). https://doi.org/10.1152/jn.00394.2017

56 Euston, D. R., Tatsuno, M. & McNaughton, B. L. Fast-forward playback of recent memory sequences in prefrontal cortex during sleep. *Science* **318**, 1147-1150 (2007). https://doi.org/10.1126/science.1148979

57 Liu, X., Leopold, D. A. & Yang, Y. Single-neuron firing cascades underlie global spontaneous brain events. *Proc Natl Acad Sci U S A* **118** (2021). https://doi.org/10.1073/pnas.2105395118

58 Yang, Y., Leopold, D. A., Duyn, J. H., Sipe, G. O. & Liu, X. Sensory Encoding Alternates With Hippocampal Ripples across Cycles of Forebrain Spiking Cascades. *Adv Sci (Weinh)* **12**, e2406224 (2025). https://doi.org/10.1002/advs.202406224

59 Gonzalo Cogno, S. *et al.* Minute-scale oscillatory sequences in medial entorhinal cortex. *Nature* **625**, 338-344 (2024). https://doi.org/10.1038/s41586-023-06864-1

60 Carrillo-Reid, L., Miller, J. E., Hamm, J. P., Jackson, J. & Yuste, R. Endogenous sequential cortical activity evoked by visual stimuli. *J Neurosci* **35**, 8813-8828 (2015). https://doi.org/10.1523/JNEUROSCI.5214-14.2015

61 Shao, S., Riquelme, J. L. & Gjorgjieva, J. Spontaneous emergence and evolution of neuronal sequences in recurrent networks. *bioRxiv*, 2024.2009.2027.615499 (2025). https://doi.org/10.1101/2024.09.27.615499

62 van der Molen, T. *et al.* Preconfigured neuronal firing sequences in human brain organoids. *Nat Neurosci* (2025). https://doi.org/10.1038/s41593-025-02111-0

63 Long, M. A., Jin, D. Z. & Fee, M. S. Support for a synaptic chain model of neuronal sequence generation. *Nature* **468**, 394-399 (2010). https://doi.org/10.1038/nature09514

64 Egger, R. *et al.* Local Axonal Conduction Shapes the Spatiotemporal Properties of Neural Sequences. *Cell* **183**, 537-548 e512 (2020). https://doi.org/10.1016/j.cell.2020.09.019

65 van Daal, R. J. J. *et al.* Implantation of Neuropixels probes for chronic recording of neuronal activity in freely behaving mice and rats. *Nat Protoc* **16**, 3322-3347 (2021). https://doi.org/10.1038/s41596-021-00539-9

66 Horan, M. *et al.* Repix: reliable, reusable, versatile chronic Neuropixels implants using minimal components. *eLife* (2024). https://doi.org/10.7554/eLife.98977.1
67 Mayerich, D., Abbott, L. & McCormick, B. Knife-edge scanning microscopy for imaging and reconstruction of three-dimensional anatomical structures of the mouse brain. *J Microsc* **231**, 134-143 (2008). https://doi.org/10.1111/j.1365-2818.2008.02024.x
68 Ragan, T. *et al.* Serial two-photon tomography for automated ex vivo mouse brain imaging. *Nat Methods* **9**, 255-258 (2012). https://doi.org/10.1038/nmeth.1854
69 Campbell, R. (Zenodo, 2020). https://doi.org/https://zenodo.org/records/3631610
70 Campbell, R., Blot, A. & Iguerard. (Zenodo, 2020). https://doi.org/https://zenodo.org/records/3941901
71 Wang, Q. *et al.* The Allen Mouse Brain Common Coordinate Framework: A 3D Reference Atlas. *Cell* **181**, 936-953 e920 (2020). https://doi.org/10.1016/j.cell.2020.04.007
72 Tyson, A. L. *et al.* Accurate determination of marker location within whole-brain microscopy images. *Scientific reports* **12**, 867 (2022). https://doi.org/10.1038/s41598-021-04676-9
73 Fabre, J. M. J., van Beest, E. H., Peters, A. J., Carandini, M. & Harris, K. D. (Zenodo, 2023). https://doi.org/https://doi.org/10.5281/zenodo.8172821
74 Kell, A. J. E. & McDermott, J. H. Invariance to background noise as a signature of non-primary auditory cortex. *Nat Commun* **10**, 3958 (2019). https://doi.org/10.1038/s41467-019-11710-y